J Mol Model (2013) 19:5407–5422
DOI 10.1007/s00894-013-2030-6

ORIGINAL PAPER

Mechanistic investigation of methanol to propene conversion catalyzed by H-beta zeolite: a two-layer ONIOM study

Yingxin Sun · Sheng Han

Received: 8 August 2013 / Accepted: 7 October 2013 / Published online: 6 November 2013

Abstract Two-layer ONIOM calculations have been carried out to study methanol to propene (MTP) conversion reactions catalyzed by H-beta zeolite. On the basis of the so-called side-chain hydrocarbon pool (HCP) mechanism, this work proposes the complete catalytic cycle pathway for the MTP reaction. The cycle starts from the methylation of pentamethylbenzene (PMB), which leads to the formation of hexamethylbenzenium ion (hexaMB$^+$). Subsequent steps involving deprotonation, methylation, an internal H-shift, and a unimolecular CH_3-shift are required to produce propene and ethene. The calculated activation barriers and reaction energy data indicate that propene is the more favored product, rather than ethene, from both kinetic and thermodynamic perspectives, which is consistent with experimental observations. In addition, the calculations suggest that the activation barriers of the reaction steps decrease in the order: internal H-shift>methylation> unimolecular CH_3-shift≥deprotonation. In the methylation step, methylation of the exocyclic double bond is easier than methylation of the ring carbons on the aromatic benzene derivative.

Keywords Methanol to propene conversion · Hydrocarbon-pool mechanism · Methylation reaction · Internal H-shift · H-beta zeolite

Electronic supplementary material The online version of this article (doi:10.1007/s00894-013-2030-6) contains supplementary material, which is available to authorized users.

Y. Sun (✉) · S. Han (✉)
School of Chemical and Environmental Engineering, Shanghai Institute of Technology, Shanghai, People's Republic of China
e-mail: sunyingxin0312@sit.edu.cn
e-mail: hansheng654321@sina.com

Introduction

Methanol can be easily and economically converted into olefins over acidic zeolites. Methanol to olefin (MTO) conversion has been one of the most prominent alternatives for the production of light olefins such as propene and ethene from crude-oil cracking [1]. Among the various MTO processes known, methanol to propene (MTP) affects the ethene/propene yield during the conversion of methanol. Propene is one of the fastest growing basic chemical intermediates in terms of demand, primarily due to the high growth rate of polypropene use [2]. The MTP process is the focus of this paper. There are at least 20 distinct proposals for the underlying mechanism of MTO or MTP catalysis in the formation of propene, ethene, or other hydrocarbon products [1]. The hydrocarbon pool (HCP) mechanism is the most likely of these; in this mechanism, organic species trapped in the pores of the zeolite are methylated repeatedly. It has become clear that polymethylbenzenes play a central role in HCP mechanism. For example, Svelle et al. investigated methanol conversion over H-beta and H-ZSM-5 zeolite catalysts under identical reaction conditions [3]. They found that, for H-beta, penta- and hexamethylbenzene are the intermediates in the HCP process, and these lead predominantly to propene and higher alkenes. However, H-ZSM-5 yields seven times more ethene relative to propene than H-beta, and lower methylbenzenes constitute the hydrocarbon pool species.

Many key experimental works on the mechanism of olefin production are reported in the literature. For example, Song et al. investigated the origins of product selectivity in MTO chemistry on HSAPO-34 zeolite [4]. They found that ethene selectivity is related to the number of methyl groups on the benzene rings trapped in the pores of zeolite. Propene is favored by tetramethylbenzene to hexamethylbenzene, but ethene is predominantly obtained from dimethylbenzene or trimethylbenzene intermediates. Sassi et al. studied the

reactions of several polymethylbenzenes such as tri-, tetra-, penta-, and hexamethylbenzene on large-pore H-beta zeolite with or without co-injection of methanol [5]. The yields of olefins increased substantially when methanol was co-reacted with polymethylbenzenes. The selectivity for propene rather than for ethene increased as the number of methyl groups on the methylbenzene increased. Bjørgen et al. reported spectroscopic evidence for a persistent benzenium cation, hexamethylbenzenium ion, on H-beta [6]. The remarkable stability of this carbenium ion can be attributed to spatial constraints imposed by the tight zeolite channels. Hexamethylbenzene is a reaction intermediate that is a hydrocarbon pool species. H-ZSM-5 zeolite is also the archetypal catalyst of the MTP process. Svelle et al. studied the formation of ethene via the conversion of methanol into hydrocarbons over H-ZSM-5 [7]. They showed that the higher methylbenzenes are present but are actually unreactive, and ethene is predominantly formed from the lower methylbenzenes.

In the present work, we focus on studying the reaction mechanisms for MTP conversion catalyzed by H-beta zeolite. Despite the great progress made over the past few decades in experimental research, a thorough atomic-level investigation is urgently required to understand the complicated MTP reaction network in detail. A theoretical approach seems warranted in this regard; indeed, perhaps it is the only choice.

Two theoretical methods have been widely used to investigate the reaction mechanism of the MTO process: the bare cluster model and periodic density functional theory (DFT). For instance, Arstad et al. studied the methylation of different methylbenzenes over a zeotype acid catalyst employing the B3LYP functional and the MP2 method in a bare cluster model [8]. They reported that methylation of methylbenzenes becomes easier as the number of methyl groups on the benzene ring increases, and predicted that heptamethylbenzenium ion could be formed. Recent experimental work has suggested that a side-chain methylation step in the HCP mechanism is plausible. Arstad et al. calculated the heats of formation of 43 alkylbenzenes in order to analyze the thermodynamics of methylation reactions using a cluster model of H-ZSM-5 zeolite [9]. Their theoretical calculations were in accord with experimental observations that selectivity for propene compared to ethene increases as the number of methyl substituents on the benzene ring increases. Vos et al. studied the alkylation reaction of toluene with methanol, which leads to the formation of three xylene isomers and is catalyzed by H-mordenite zeolite, using periodic DFT [10]. Their calculations showed that steric constraints in zeolite have a significant effect on the activation energy for methylation, such that *para* < *ortho* < *meta* (whereas *ortho* < *para* < *meta* in the absence of steric constraints). Wang et al. proposed the first complete catalytic cycle for the MTO reaction via hexamethylbenzene encapsulated in HSAPO-34 zeolite based on periodic DFT calculations [11]. Their results suggested that the hexamethylbenzene on the HSAPO-34 only produces propene as the primary product. Propene and ethene were obtained from the elimination of the side isopropyl and ethyl groups on the benzenium ions, respectively.

The bare cluster approach, in which the zeolites are represented by small silicon oxide clusters, is useful for describing local catalytic reactions near active acidic sites, but this approach makes it difficult to understand the effect of the zeolite environment. The periodic DFT method is computationally too expensive when very large zeolites are involved. Recently, a quantum mechanical/molecular mechanical (QM/MM) method [12–14] as well as the more general ONIOM (Our-own-N-layered Integrated molecular Orbital+molecular Mechanics) scheme have been proposed [15–17]. The QM/MM scheme combines the advantages of the high accuracy of quantum chemistry calculations and the high efficiency of using a molecular mechanics force field to represent long-range interactions. For example, Lesthaeghe et al. investigated the methylation of several methylbenzenes such as toluene, pentamethylbenzene (PMB), and hexamethylbenzene (HMB) in the acidic BEA, CHA, and MFI zeolite topologies using a 5T cluster and the ONIOM model [18]. The results calculated with the 5T cluster suggest a steady decrease in activation barrier and reaction energy as the number of methyl groups on the benzene ring of the methylbenzene increases. The topology of the zeolite affects the reaction kinetics. The following order of reactivity was observed when using the ONIOM method: CHA >>MFI> BEA. Recently, utilizing experimental kinetic measurements and ONIOM calculations, Mynsbrugge et al. studied the methylation of benzene by methanol on H-ZSM-5 and H-beta zeolites in order to investigate the effect of zeolite topology on the reaction rate [19]. The calculated results reproduced the experimentally observed higher rate of methylation in H-ZSM-5 and suggested that this may be attributed to stronger co-adsorption of benzene molecules in the smaller pores of H-ZSM-5 than in those of H-beta. One of the successful applications of our previous work was an ONIOM(MP2//DFT:UFF) investigation of the initial reactions involved in the catalytic cracking of 1-butene to produce propene and ethene over H-ZSM-5 and H-FAU zeolites [20].

In the work described in the present paper, we performed a detailed theoretical study of the reaction mechanism of methanol to propene conversion catalyzed by H-beta zeolite, performed using the two-layer ONIOM approach. We aimed to address the following two interesting questions. (1) What are the elementary steps involved in the complete catalytic cycle for the MTP process? (2) How are propene and ethene produced, and what is the rate-determining step? The present calculations should prove useful for optimizing the reaction conditions and when designing more efficient catalysts for industrial production.

Computational details

An extended 188T nanocluster covering the active region of the H-beta zeolite was used to represent the Brønsted acid site and the zeolite framework in this work. The atomic coordinates of this model were taken from lattice data for the H-beta cell with space group $P4_122$ ($a=b=12.661$ Å, $c=26.406$ Å, $\alpha=\beta=\gamma=90.0°$) [21]. Figure 1 illustrates the 188T model, which includes a 12-membered ring (12MR) representing the main gateway to the intersection of two perpendicular 12MR channels A and B. An Si atom at the T5 position in the H-beta is replaced with an Al atom. A proton is attached to the bridging oxygen atoms that are bonded directly to the Al atom (this is conventionally called the O5 position, but is designated the Oa position in this study). The acidic proton may also be transferred to the Ob, Oc, and Od positions. Among these, Oa and Ob were chosen as the most likely proton positions, as they have lower energies than the Oc and Od positions (see the "Electronic supplementary material," ESM, Table S1). The dangling bonds that result from cutting the external Si–O bonds were saturated with hydrogen atoms, with the Si–H bond distances fixed at 1.470 Å.

We applied a two-layer ONIOM scheme in all calculations. In this method, the total ONIOM energy of the system is obtained from the following equation [22]:

$$E_{\mathrm{ONIOM2}} = E_{\mathrm{MM}}^{\mathrm{All}} - E_{\mathrm{MM}}^{\mathrm{Inner}} + E_{\mathrm{QM}}^{\mathrm{Inner}}, \quad (1)$$

where the "all" region includes an "inner" region and a large "outer" region. The outer region was the extended zeolite framework and was only treated at the molecular mechanics (MM) level. The inner region, which contained the active Brønsted acidic site and reacting species, was calculated at the quantum mechanics (QM) level. Both QM and MM calculations had to be performed for the inner system. In this scheme, the van der Waals (VDW) and electrostatic interaction energies were evaluated via the MM terms.

An S value test can be used to check the errors associated with the ONIOM extrapolation method. Since the ONIOM energy surface is continuous, the MM contribution to the

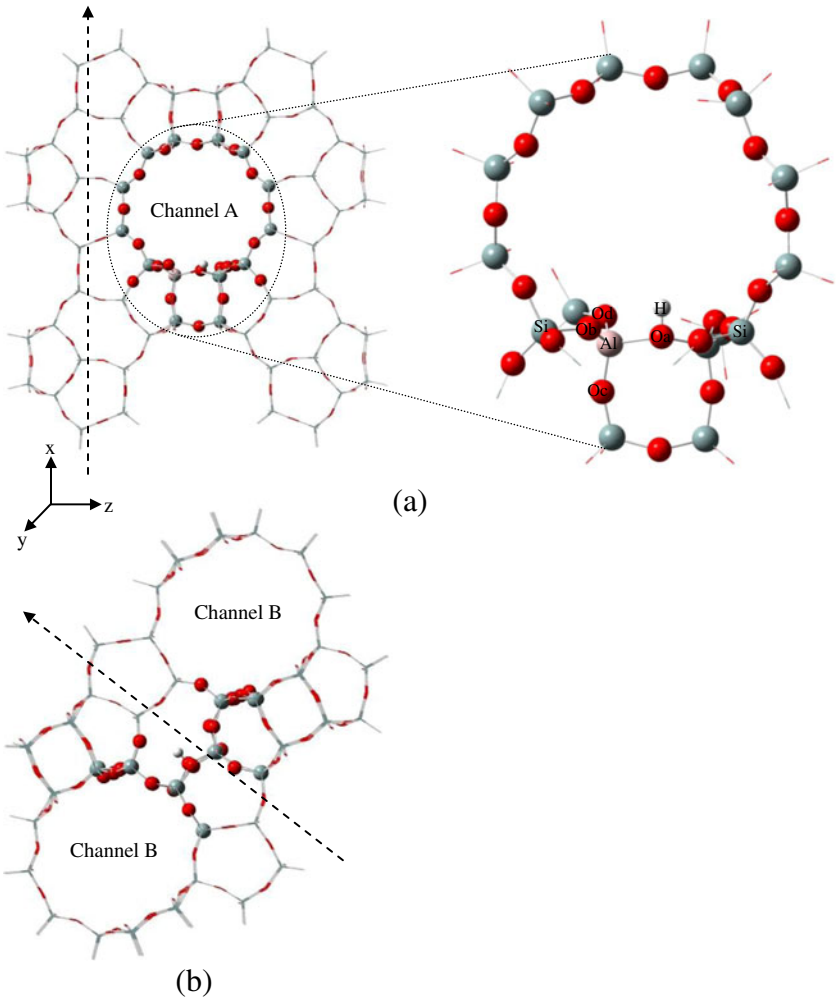

Fig. 1 188T nanocluster model of H-beta zeolite divided into two regions: the inner 16T region (indicated by *colored balls*) is described using quantum mechanics, and the outer region is described using UFF. **a** Front view; the *oval dashed line* encloses the 16T active region where the MTP reaction takes place. **b** Side view. The *arrow* indicates the direction of channel B (in **a**) or A (in **b**)

ONIOM energy must be continuous. The MM contribution is defined as the S value [17, 23], i.e.,

$$S^{MM} = E_{MM}^{All} - E_{MM}^{Inner}. \quad (2)$$

The S value must be independent of the definition of the connectivity for each intermediate and transition state (TS) structure involved in reaction pathways. For instance, for each transition state structure of MTP reaction, the S value calculated with the connectivity as in the reactant structure must be the same as the S value calculated with the connectivity as in the product structure. We calculated several representative transition states of the MTP process on H-beta zeolite and found that the differences in S value between different choices of connectivity were zero. The corresponding data are summarized in Table S2 in the ESM.

In the ONIOM calculations, we employed the M06-2X hybrid meta-GGA functional [24–27] and the universal force field (UFF) [28] to describe the inner and outer regions, respectively. It is well known that the B3LYP functional [29] underestimates the activation barriers of transition states and is not appropriate for describing medium-range van der Waals interactions. The M06-2X functional, as developed by Zhao and Truhlar et al., was proposed in order to solve these problems, and shows promising performance when studying main-group thermochemistry, excited states, kinetics, noncovalent interactions, and transition elements. To save computing time, the inner QM region was further divided into two subregions that were treated using mixed basis sets. An active subregion that included an 8T cluster of the active site of zeolite and reacting species was treated using the 6-31G(d,p) basis set; the other 8T cluster of the inner region was treated using the 3-21G basis set. This combination rule was called M06-2X(8T(6-31G(d,p)) : 8T(3-21G)). The complete zeolite system was called ONIOM(M06-2X(8T(6-31G(d,p)) : 8T(3-21G)):UFF) or ONIOM(16T:188T). According to previous work, the 16T QM cluster is considered large enough that it can be effectively used to study the present reaction mechanism over H-beta zeolite [30]. During geometry optimizations, only the 5T region [(≡SiO)$_3$Al(OH)Si≡] and the reacting molecules were allowed to relax, while the rest of the 188T model was fixed along the crystallographic coordinates. Frequency calculations were used to characterize each stationary point as either an intermediate (zero negative frequency) or a transition state (exactly one negative frequency). To obtain more reliable interaction energies, single-point energy calculations were carried out at the M06-2X(8T(6-311+G(2df,2p)) : 8T(6-31G(d,p))) and MP2(8T(6-311+G(d,p)) : 8T(6-31G(d,p))) levels, based on the abovementioned optimized structures for the QM regions. The latter scheme was denoted MP2//M06-2X. The corresponding ONIOM(MP2//M06-2X:UFF) energy values are referred to when energies are discussed in this paper. For analytical convenience, the total ONIOM energy data were decomposed into QM and MM contributions.

Since the charge parameters are not optimized for zeolite systems in the UFF force field, we calculated the electrostatic potential (ESP) energy of a 102T pure silica zeolite model via M06-2X/6-31G(d,p) single-point calculations and obtained charge values for the MM region by fitting the ESP energy. The charge values for the QM region were taken directly from the ESP charges in DFT calculations performed with the M06-2X functional using the ChelpG scheme [31] for each intermediate and transition state structure around the active sites of the zeolites. The charge distribution was subject to charge neutrality constraints in the QM and MM regions. Electrostatic interactions between the QM and MM regions were calculated using a mechanical embedding scheme that has been applied successfully to reaction mechanisms many times [32–34]. For comparison, geometry optimization was performed both with and without MM charges. All calculations in this work were performed using the Gaussian 09 software package [35].

Results and discussion

Based on previous experimental and theoretical work [1], we were able to propose the reaction mechanism for the MTP process on H-beta zeolite after identifying the related intermediates and transition states in the elementary steps. The proposed pathway is summarized in Scheme 1, and the corresponding energy profile is given in Fig. 2. Note that all of the energy values were calculated as follows: for each intermediate or transition state, energy data were calculated relative to the total energy of the reactant molecules (methanol and PMB) and H-beta zeolite at infinite separation; for transition states, the activation barriers were obtained as the difference in energy between the transition state and the previous intermediate.

The PMB and HMB are organic active centers for the growth of the C–C chain through the so-called side-chain HCP mechanism. PMB can be converted into HMB through methylation and subsequent deprotonation steps. The products, propene and ethene, are eliminated from the side chain of the aromatic benzene derivative by an internal H-shift step. Two different pathways have been reported for the methylation step in the literature [36–38]: a stepwise mechanism that involves a surface-bound methoxide intermediate, and a concerted one in which adsorbed methanol directly attacks the substrate to be methylated. The concerted pathway is widely used in theoretical calculations because the experimental kinetic measurements are readily explained by this pathway [19, 37, 39], so we adopted this mechanism in the present work. In the following, we discuss our calculated results (as reported in Scheme 1 and Fig. 2) in detail.

Scheme 1 The proposed mechanism for the MTP process in acidic H-beta zeolite

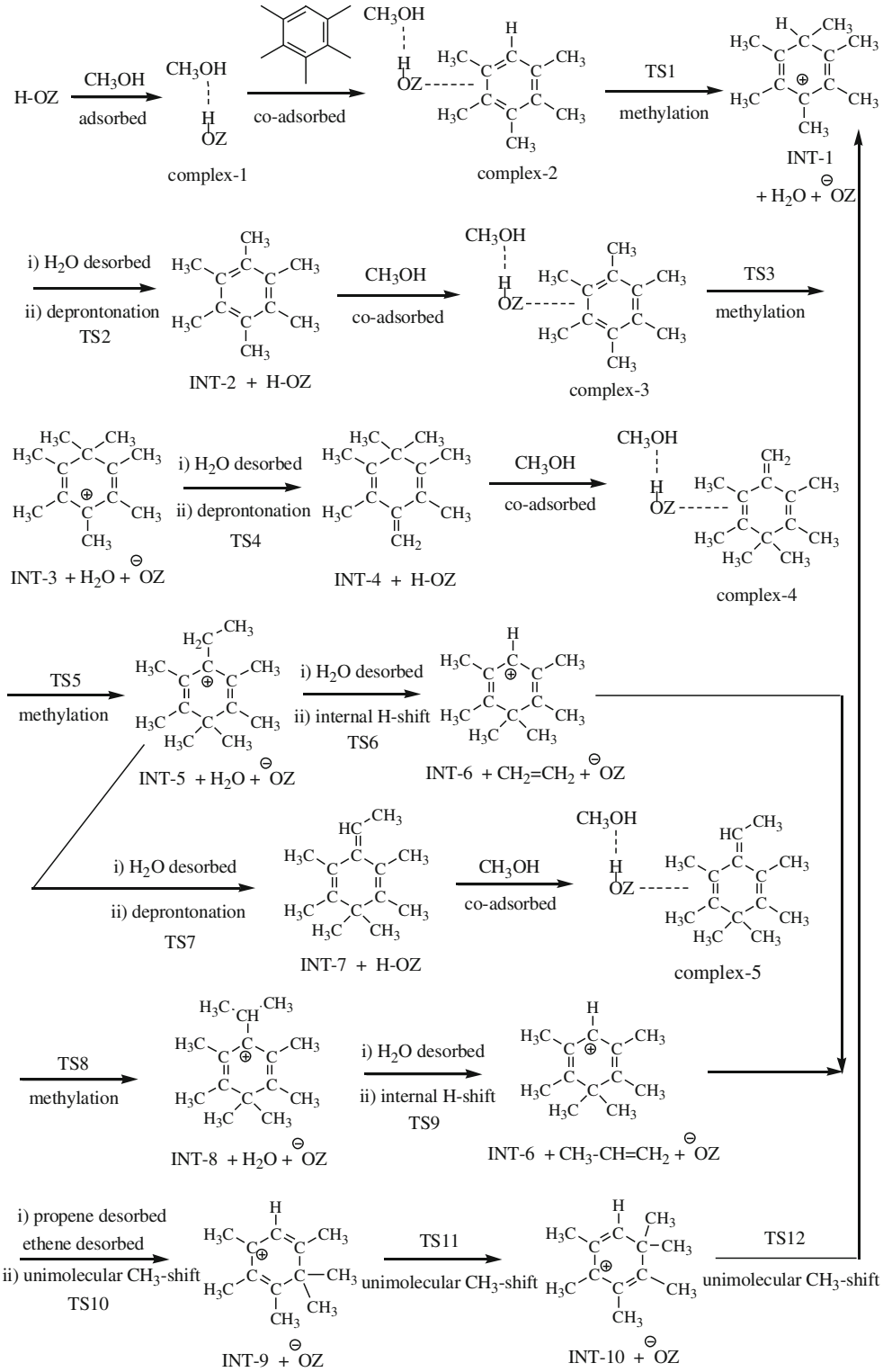

Formation of hexamethylbenzene (HMB)

The initiating step in the MTP reaction is the capture of methanol by the Brønsted acid site of H-beta through the formation of two hydrogen bonds (complex-1), as shown in Fig. 3a. The first H-bond is between the acidic proton of zeolite and the oxygen in methanol. This interaction is strong because of the short ZOH…$OHCH_3$ distance of 1.312 Å. The other H-bond is between the hydroxyl proton in methanol and the oxygen in zeolite, which has a bond length of

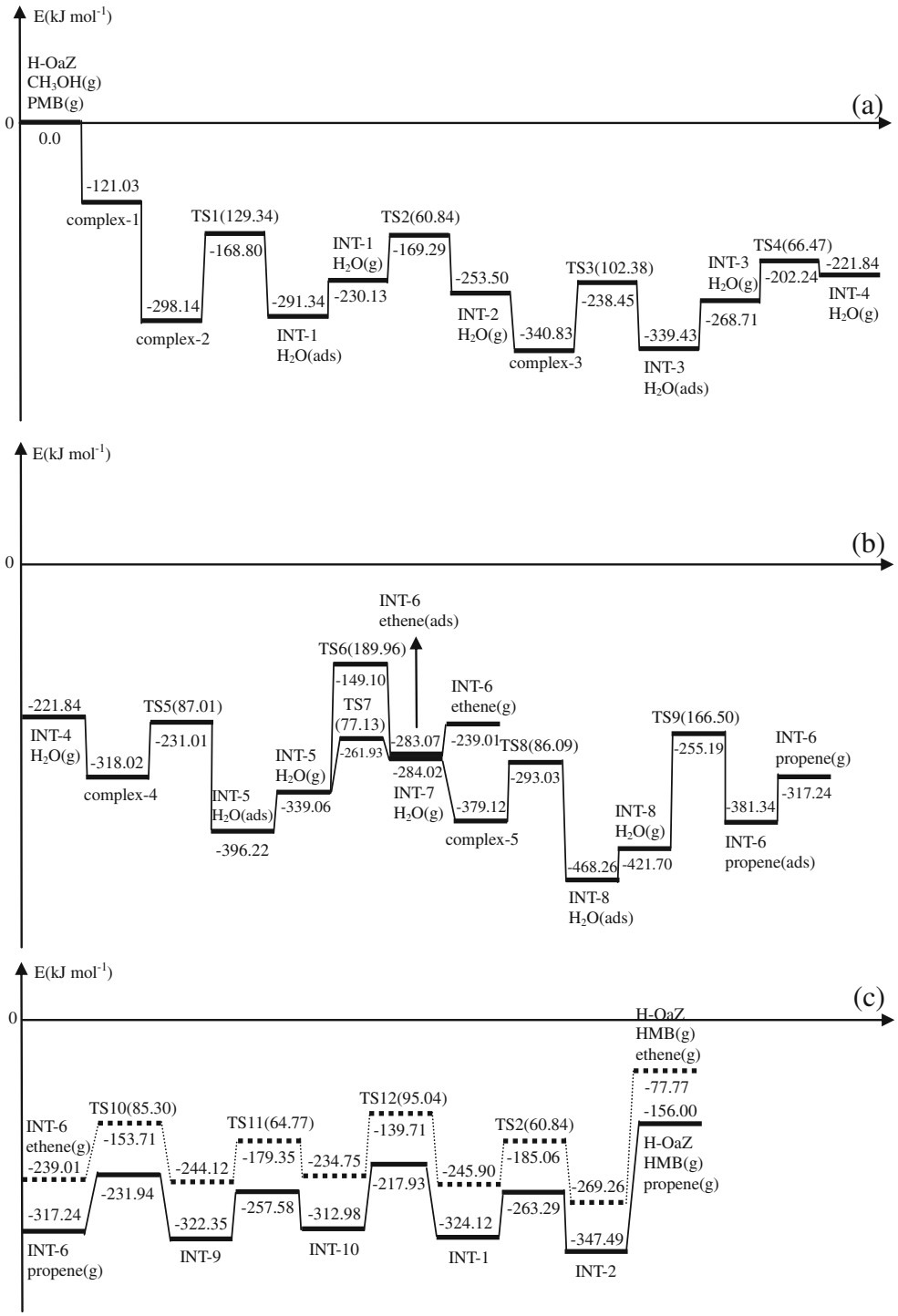

Fig. 2 Energy profiles calculated for the MTP reaction pathway illustrated in Scheme 1. Energy data for each species were calculated relative to the total energy of the reactants (methanol and PMB) and H-beta zeolite at infinite separation. For transition states, the activation barriers ΔE_{act} are given in *parentheses*, i.e., TSn(ΔE_{act})

1.906 Å. The zeolite Oa–H bond length of 1.113 Å is longer than the isolated Oa–H bond length of 0.972 Å. The adsorption configuration is similar to that described by Svelle (hybrid MP2:DFT method, H-ZSM-5 [40]), Mynsbrugge (ONIOM(DFT:MNDO), H-beta [19]), and Wang (DFT, HSAPO-34 [11]). The adsorption energy of methanol is −121.03 kJ mol^{-1} when calculated at the MP2 level, as compared to the values of −111 (ωB97X-D) and −120 (B3LYP-D3) kJ mol^{-1} predicted by Mynsbrugge et al. using the ONIOM(10T:52T) model [19]. Detailed analysis of the energy components in Table 1 suggests that most of the adsorption energy of methanol derives from the QM contribution. However, the MM contribution from the van der Waals (VDW) and electrostatic interactions are not negligible (they account for 16 % of the total adsorption energy). It should be noted that the adsorption energy of

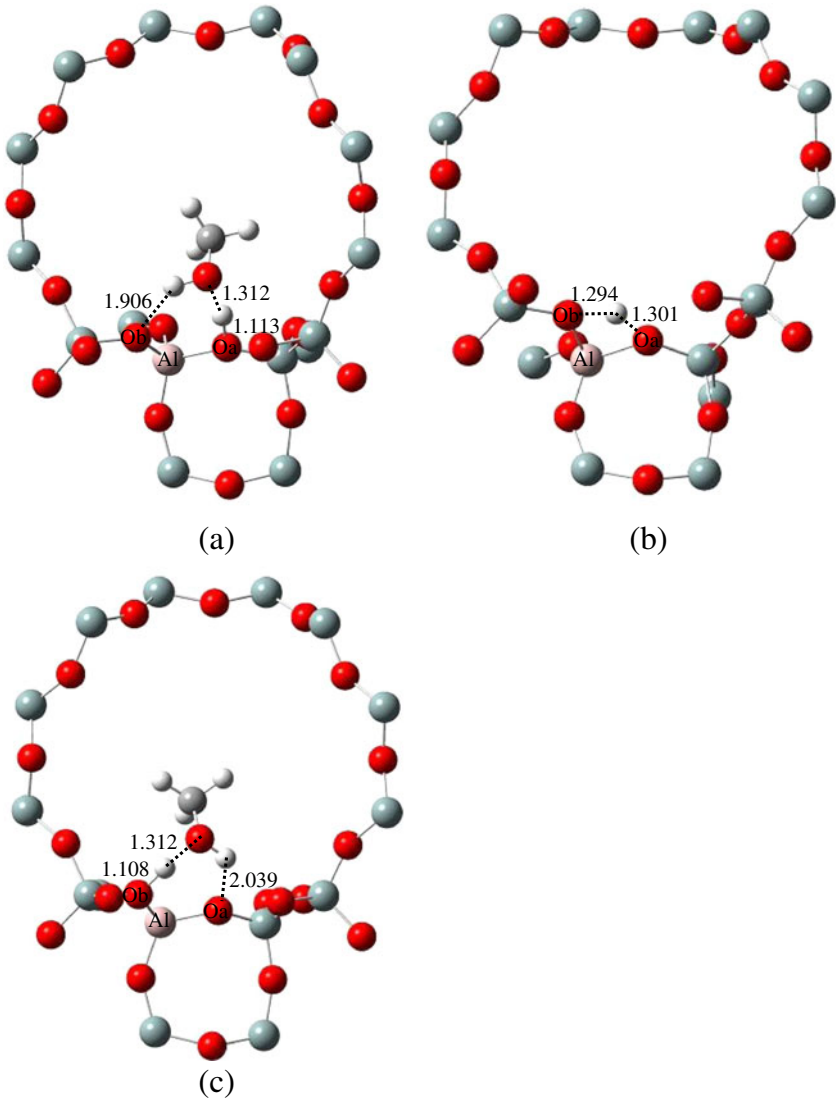

Fig. 3 Optimized structures of **a** complex-1, **b** TS_{trans}, **c** complex-1′

methanol calculated using the M06-2X functional is −108.95 kJ mol^{-1}, suggesting that MP2 electron correlation enhances the nonbonded interactions and yields the lowest of the adsorption energies mentioned above (−121.03 kJ mol^{-1}).

Table 1 Adsorption energies (kJ mol^{-1}) of methanol at the Oa and Ob positions, showing QM and MM contributions

	QM	MM	ONIOM	Literature
Complex-1	−101.13 (−89.04)[a]	−19.90	−121.03 (−108.95)	−111[b], −120[c]
Complex-1′	−117.32 (−106.86)	−21.46	−138.77 (−128.31)	

[a] The energy values in parentheses were obtained at the M06-2X level of theory

[b] Value obtained at the ωB97X-D level; see [19]

[c] Value obtained at the B3LYP-D3 level; see [19]

Interestingly, the acidic proton can be transferred from the Oa to the Ob position. For this proton jump to occur, an activation barrier of 139.75 kJ mol^{-1} must be surmounted, and the resulting step is endothermic by 20.59 kJ mol^{-1}. Figure 3b shows the corresponding transition state structure (TS_{trans}). In TS_{trans}, the H–Oa and H–Ob distances are nearly equal (1.301 vs. 1.294 Å). This transfer process is unfavorable, but the adsorption energy of methanol at the Ob position (Fig. 3c, complex-1′) is 17.74 kJ mol^{-1} larger than that at the Oa position (see Table 1). The difference between the methanol adsorption energies at different oxygen positions is mainly due to the QM contribution. Structural analysis of the hydrogen bonding for these two methanol adsorption configurations clearly indicates that the methanol is not protonated, which is consistent with previous studies on H-ZSM-5 and H-beta [19, 40]. Further manual geometry optimization does not locate this stationary point for protonated methanol on the potential energy surface.

In the ensuing steps, a PMB molecule inside the zeolite cage is co-adsorbed onto the methanol complex (complex-2) and subsequently methylated through an S_N2-type transition state (TS1). After TS1, the hexamethylbenzenium ion (hexaMB$^+$, INT-1) and an H_2O molecule are produced. The corresponding intermediate and TS1 structures are shown in Fig. 4. At TS1, the hydroxyl group on methanol is almost fully protonated by the acidic proton of zeolite, because the two O–H distances in H_2O are nearly 0.976 Å and the length of the O–C bond that breaks is very long: 2.141 Å (the O–C distance in methanol is 1.440 Å). The central methyl group is essentially cationic and almost planar. The C–C bond that forms is 2.116 Å in length, and the O–C–C angle is about 163.670°. An activation barrier of 129.34 kJ mol^{-1} must be overcome for this methylation step to occur, and the step itself is endothermic by 6.80 kJ mol^{-1} (Fig. 2a). Table 2 lists the energy values obtained at different levels of theory. We analyzed the activation barrier in terms of QM and MM components. The small MM energy contribution of −9.37 kJ mol^{-1} implies that the nonbonded energies of TS1 and complex-2 are similar.

Several conclusions can be drawn from Table 2. First, the effect of electrostatic interactions on the MM contribution is small for complexes but very important for transition states. For example, the MM energies with and without charge interactions for the adsorption energy of complex-2 are −88.35 and −85.46 kJ mol^{-1}, respectively. However, for the activation barrier of TS1, the corresponding MM energies are −9.37 and 7.93 kJ mol^{-1}, respectively, indicating that different nonbonded interactions are present. This result is easily understood if we note that the transition states are charged species but the complexes are neutral.

Second, the MP2 correlation energies yield larger adsorption energies and lower activation barriers. For example, upon changing from using the M06-2X functional to employing the MP2 method, the adsorption energy of PMB increases by 29.80 kJ mol^{-1} and the activation barrier of TS1 decreases by 20.82 kJ mol^{-1}.

The formed hexaMB$^+$ ion can lose its proton from the aromatic carbon to the oxygen atom in the framework of H-beta (TS2), which yields the intermediate HMB, as shown in Fig. 5 (INT-2). At TS2, the Oa–H and H–C bond distances are 1.508 and 1.312 Å, respectively. In INT-2, the

Table 2 Adsorption energies (kJ mol^{-1}) of PMB in complex-2 and activation barriers of TS1 (kJ mol^{-1}) for the methylation of PMB calculated at different levels of theory, showing QM and MM contributions

	Level of theory	PMB	TS1
ONIOM	QM(MP2-SPE)[c]	−88.76	138.72
(VDW+charge)[a]	QM(M06-2X-SPE)[d]	−58.96	159.53
	MM	−88.35	−9.37
	ONIOM(MP2-SPE[f]:UFF)	−177.11	129.34
	ONIOM(M06-2X-SPE:UFF)	−147.31	150.16
ONIOM	QM(M06-2X-OPT)	−41.69	167.72
(VDW only)[b]	MM	−85.46	7.93
	ONIOM(M06-2X-OPT:UFF)[e]	−127.15	175.65

[a] MM energy terms include the van der Waals and electrostatic interaction energies

[b] MM energy terms include the van der Waals interactions only

[c] MP2 single-point energy calculations performed at the MP2(8 T(6-311+G(d,p)):8T(6-31G(d,p))) level for the QM region

[d] M06-2X single-point energy calculations performed at the M06-2X(8T(6-311+G(2df,2p)):8T(6-31G(d,p))) level for the QM region

[e] M06-2X geometry optimizations performed at the ONIOM(M06-2X(8T(6-31G(d,p)):8T(3-21G)):UFF) level without MM charges

[f] The abbreviation *SPE* refers to the single-point energy

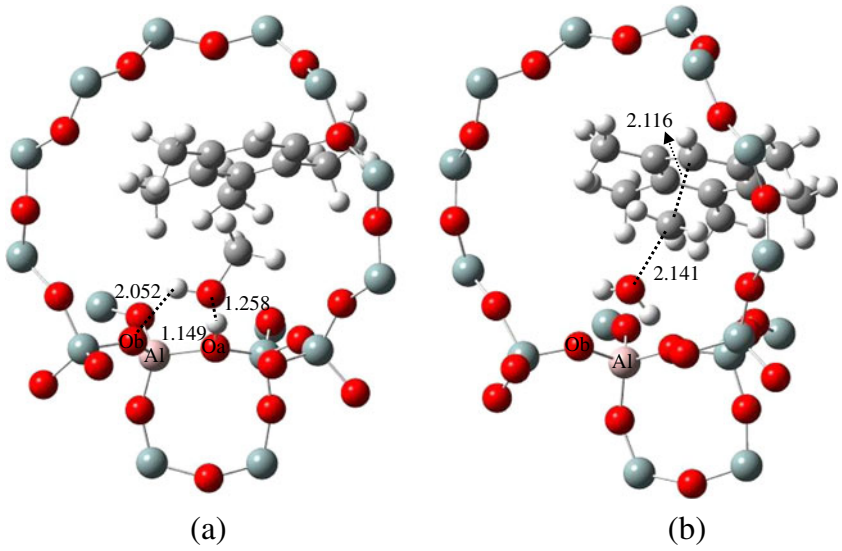

Fig. 4 Optimized structures of **a** complex-2 and **b** TS1

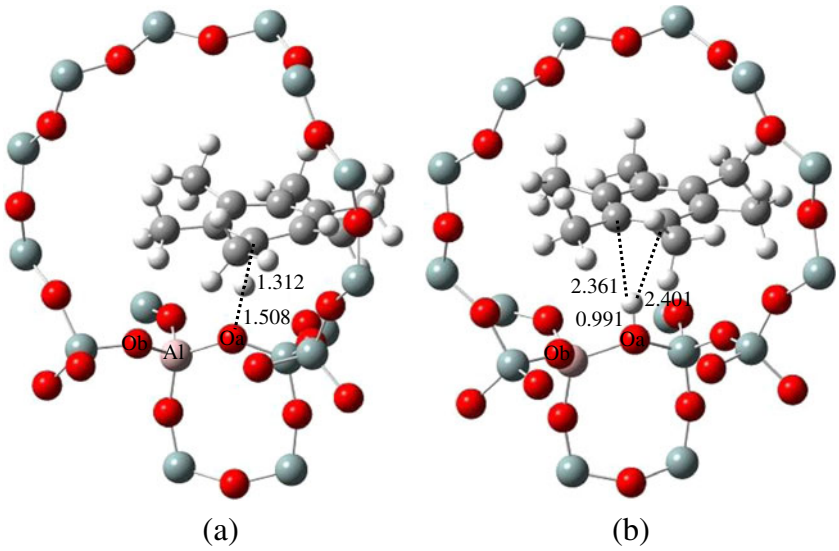

Fig. 5 Optimized structures of **a** TS2 and **b** INT-2

distance between the acidic proton and the two nearest aromatic carbon atoms on HMB is about 2.40 Å. The calculated reaction barrier for the deprotonation of hexaMB$^+$ is 60.84 kJ mol^{-1} (Fig. 2a). The reverse step, the protonation of HMB, has an activation barrier of 84.20 kJ mol^{-1}, and is endothermic by 23.37 kJ mol^{-1}. PMB and HMB are important hydrocarbon pool species for the growth of the C–C chain via the side-chain HCP mechanism.

Formation of 1,1,2,3,5,6-hexamethyl-4-ethylbenzenium ion (INT-5)

The subsequent step is the methylation of HMB, which begins with the co-adsorption of methanol onto the HMB complex (complex-3). The adsorbed methanol can attack HMB through the transition state TS3 to form the heptamethylbenzenium ion (heptaMB$^+$, INT-3) and an H_2O molecule. Figure 6 shows the structures of complex-3 and TS3. The methanol in complex-3 can be considered a protonated methanol ($CH_3OH_2^+$) with two almost equally long O–H distances of 1.048 and 1.058 Å. The Oa–H and Ob–H distances are 1.449 and 1.406 Å, respectively. At TS3, the breaking O–C bond is 2.111 Å and the forming C–C bond is 2.007 Å in length, while the O–C–C angle is 162.255°. The structure of TS3 is very similar to that of TS1. The calculated barrier energy and reaction energy are 102.38 and 1.40 kJ mol^{-1}, and the corresponding QM and MM contributions are listed in Table S3 of the ESM. The low MM energy is compensated for by the high QM energy, which reflects the compromise between the strong nonbonded interactions and high spatial hindrance of large aromatic molecules. Lesthaeghe et al. investigated the methylation of several methylbenzenes, including HMB species, at the ONIOM(B3LYP/6-31+G(d): HF/6-31+G(d))//ONIOM(B3LYP/6-31+G(d):MNDO) level of theory [18]. They predicted a reaction barrier of 144.0 kJ mol^{-1} for the methylation of HMB on H-beta. Our result, calculated at the ONIOM(M06-2X(8T(6-31G(d,p)) : 8T(3-21G)):UFF) level, is 144.54 kJ mol^{-1}, which is in accord with the value mentioned above, indicating that MP2 electron correlation reduces the activation barrier.

The formed heptaMB$^+$ can lose the proton from its side-chain methyl group to the framework of H-beta, leading to the formation of the olefin hexamethylmethylenecyclohexadiene (HMMC, INT-4) by a deprotonation step (TS4). The corresponding reaction barrier is 66.47 kJ mol^{-1}, but the protonation of HMMC has an energy barrier of 19.60 kJ mol^{-1} as well as a reaction energy of −46.87 kJ mol^{-1}. This result indicates that HMMC and heptaMB$^+$ are in a state of equilibrium, which is consistent with the results of a related experimental study [41]. The energy data are decomposed into QM and MM contributions in Table S4 of the ESM. One can conclude that most of the activation barrier comes from the QM contribution, whereas the MM contribution accounts for more than half of the reaction energy. Figure 7 shows the intermediate and transition state structures. Going from HMMC to TS4, the Oa–H bond is elongated from 0.999 to 1.288 Å and the exocyclic double-bond distance increases from 1.360 to 1.402 Å, which leads to the formation of the heptaMB$^+$ ion (INT-3). Recently, for the first time, Li et al. observed the heptaMB$^+$ ion directly under real working conditions on the DNL-6, a newly synthesized SAPO-type molecular sieve with large cavities [42].

The next step is the methylation of HMMC. After the formation of complex-4, the adsorbed methanol can attack the exocyclic double bond of HMMC to form a side ethyl group through transition state TS5, which produces the intermediate 1,1,2,3,5,6-hexamethyl-4-ethylbenzenium ion (INT-5). The structures of complex-4 and TS5 are given in Fig. 8. The methanol in complex-4 has been protonated to form the $CH_3OH_2^+$ structure, with two O–H distances of

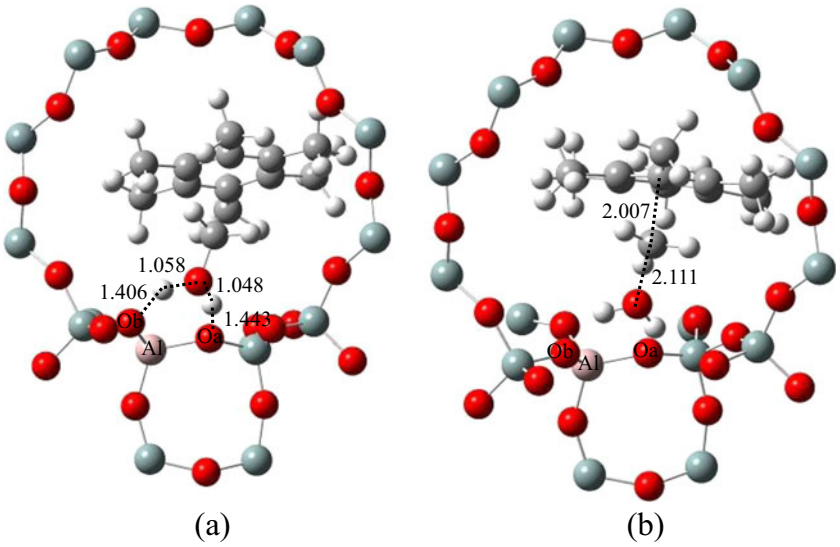

Fig. 6 Optimized structures of **a** complex-3 and **b** TS3

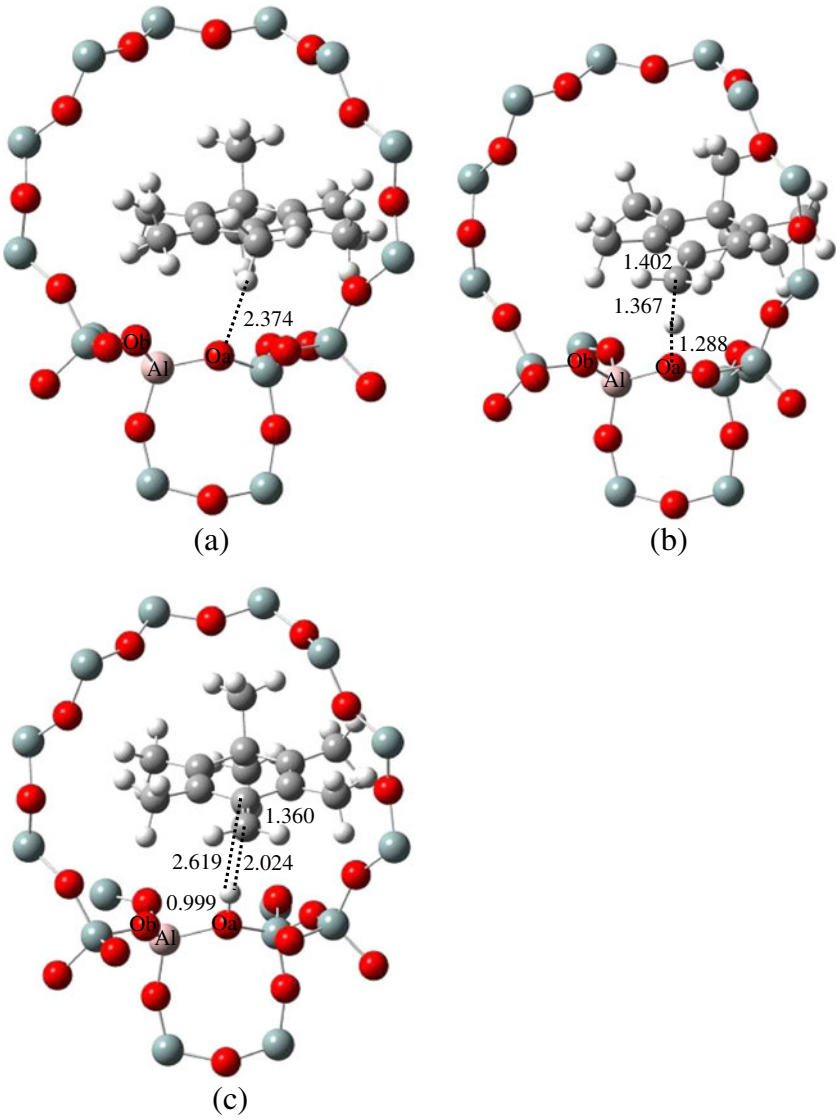

Fig. 7 Optimized structures of **a** INT-3, **b** TS4, and **c** INT-4

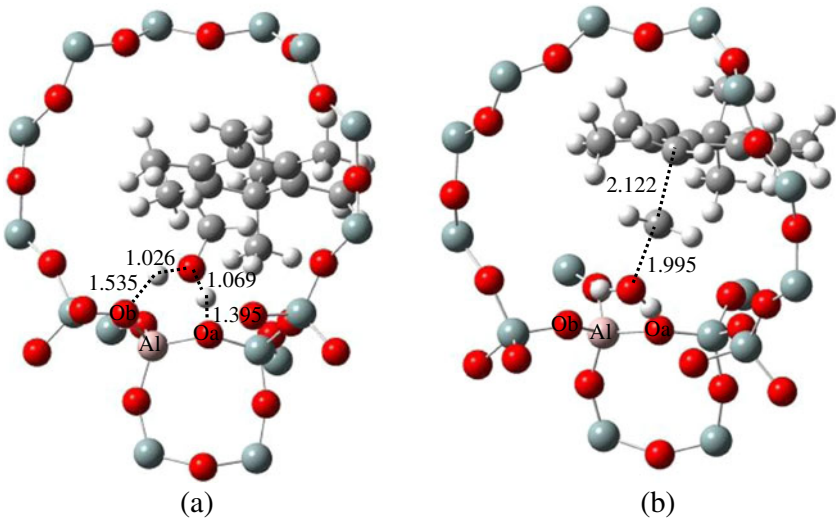

Fig. 8 Optimized structures of **a** complex-4 and **b** TS5

1.026 and 1.069 Å. The lengths of the two hydrogen bonds Oa–H and Ob–H are 1.395 and 1.535 Å, respectively. The configuration of complex-4 is similar to that of complex-3. At TS5, the lengths of the breaking O–C bond and the forming C–C bond are 1.995 Å and 2.122 Å, respectively, while the O–C–C angle is 169.467°. The structure of TS5 is very similar to those of TS1 and TS3.

The methylation of HMMC has an activation barrier of 87.01 kJ mol^{-1} and is exothermic by −78.20 kJ mol^{-1} (Fig. 2b). The low MM contribution of −23.72 kJ mol^{-1} to the total ONIOM activation barrier is compensated for by the high QM energy of 110.73 kJ mol^{-1}, reflecting both the increase in the strength of nonbonded interactions and the increase in intramolecular tension upon moving from complex-4 to TS5. Upon comparing it with the methylation of HMB, one can see that the methylation of the exocyclic double bond is easier than the methylation of the aromatic ring carbon atoms (C_{ring}), which is probably due to the greater spatial hindrance at the C_{ring} position of HMB. This result is in accord with those obtained in previous theoretical studies on HSAPO-34 zeolite, as reported by Wang et al. [11]. The small activation barrier of TS5 indicates that the methylation of HMMC is not the rate-determining step for the MTP process. Starting from the intermediate INT-5, propene and ethene can be produced through deprotonation, methylation, and internal H-shift steps.

Production of propene and ethene

Ethene can be produced by shifting one end H atom in the side ethyl group of INT-5 to the C_{ring} atom through a direct internal H-shift transition state TS6. After TS6, the ethene and an intermediate, the 1,1,2,3,5,6-hexamethylbenzenium ion (INT-6), are formed. The calculated activation barrier for this process is high, 189.96 kJ mol^{-1}, and the process is endothermic by 55.98 kJ mol^{-1} (Fig. 2b). Analysis of the energy components suggests that the high reaction barrier is mainly due to the QM contribution. The structures of INT-5, TS6, and INT-6 are given in Fig. 9. At TS6, the breaking C–H bond in the CH_3 group is elongated to 1.813 Å and the C–C distances between the ethyl group and the ring carbon are 1.750 and 1.837 Å. The ethene and INT-6 are co-adsorbed near the active site. This H-shift step is rate-determining for the production of ethene.

When propene is produced, the olefin 1,2,3,3,4,5-hexamethyl-6-ethylidene-1,4-cyclohexadiene (HMEC, INT-7) with an exocyclic double bond is first formed via the deprotonation of INT-5, which has an activation barrier of 77.13 kJ mol^{-1} (TS7) and a reaction energy of 55.04 kJ mol^{-1}. The methylation of HMEC (to form TS8) by a fourth adsorbed methanol can propagate the exocyclic side chain, leading to 1,1,2,3,5,6-hexamethyl-4-isopropylbenzenium ion (INT-8). The calculated activation barrier of 86.09 kJ mol^{-1} for TS8 is similar to that for TS5 (83.60 kJ mol^{-1}), mainly because these two steps involve the same methylation of the exocyclic double bond. Similarly, the difference in the activation barriers for TS7 (77.13 kJ mol^{-1}) and TS4 (66.47 kJ mol^{-1}) is small because both steps involve a deprotonation step and the formation of the exocyclic double bond. TS7, INT-7, complex-5, and TS8 are all shown in Fig. S1 of the ESM. Careful analysis of their structures suggests that the structure of TS8 is similar to those of TS1, TS3, and TS5. Moreover, TS7 and TS4 are structurally similar. The methanol in complex-5 can be considered to be the protonated species $CH_3OH_2^+$, similar to those in complex-3 and complex-4.

We investigated the abovementioned similarities between the different transition states, and the results are shown in Tables 3 and 4. In Table 3, TS2, TS4, and TS7 all involve a deprotonation step to form the exocyclic double bond on the

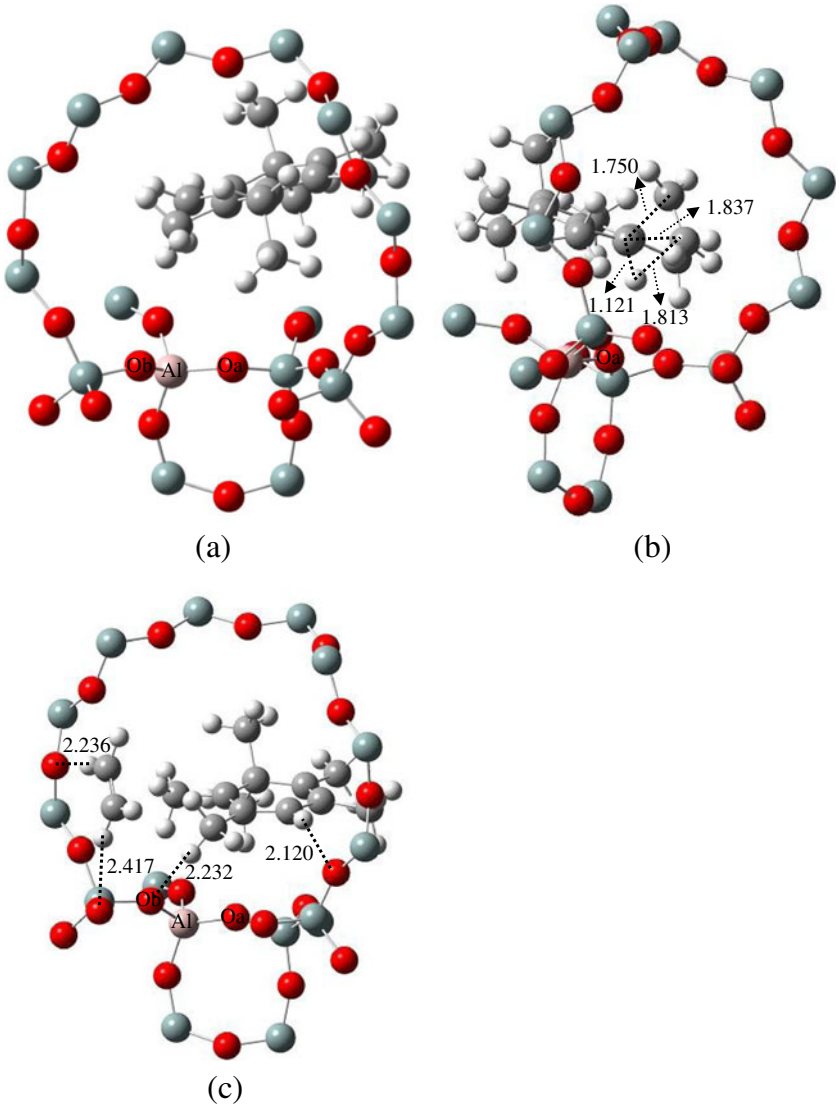

Fig. 9 Optimized structures of **a** INT-5, **b** TS6, and **c** INT-6 with ethene

aromatic benzene derivative. TS7 has a higher activation barrier than TS4 does mainly because of the MM contribution and the greater spatial hindrance of TS7. The lower activation barrier for TS2 than for TS4 probably originates from the higher degree of conjugation of the HMB fragment of TS2.

Table 3 Activation barriers (kJ mol^{-1}) for the deprotonation steps of TS2, TS4, and TS7, showing QM and MM contributions

	QM	MM	ONIOM
TS2	42.23 (50.97)[a]	18.61	60.84 (69.58)
TS4	49.89 (54.51)	16.58	66.47 (71.09)
TS7	47.57 (59.97)	29.56	77.13 (89.53)

[a] Energy values in parentheses were obtained at the M06-2X level

Table 4 gives energy data on TS1, TS3, TS5, and TS8. These four transition states are structurally similar but have different activation barriers. For the methylation process, the smaller spatial hindrance of the exocyclic double bond compared to that afforded by the aromatic carbon on the benzene ring leads

Table 4 Activation barriers (kJ mol^{-1}) for the methylation steps of TS1, TS3, TS5, and TS8, showing QM and MM contributions

	QM	MM	ONIOM
TS1	138.72 (159.53)[a]	−9.37	129.34 (150.16)
TS3	118.18 (139.41)	−15.81	102.38 (123.61)
TS5	110.73 (122.50)	−23.72	87.01 (98.78)
TS8	109.63 (124.83)	−23.54	86.09 (101.29)

[a] Energy values in parentheses were obtained at the M06-2X level

to lower activation barriers for TS5 and TS8 than for TS1 and TS3. Furthermore, the greater electron density on benzene of HMB than on PMB means that the activation barrier of TS3 is lower than that of TS1.

An internal H-shift in INT-8 occurs to produce the propene and INT-6 through the transition state TS9, as shown in Fig. 10. At TS9, the breaking C–H bond of the CH_3 group is elongated to 1.597 Å and the C–C distance between the isopropyl group and the ring carbon is 1.658 Å. After TS9, the propene is desorbed as a product and the INT-6 participates in subsequent methyl shift reactions, allowing catalytic cycle completion. The H-shift step has an energy barrier of 166.50 kJ mol^{-1} and is endothermic by 40.35 kJ mol^{-1}. This step is rate-determining for the production of propene. Table 5 lists the total ONIOM energies and the energy components of the rate-determining steps associated with TS6 and TS9. The MM contribution accounts for 11 % (TS6) and 12 % (TS9) of the total activation barrier, respectively.

Table 5 Activation barriers (kJ mol^{-1}) of TS6 and TS9 and reaction energies (ΔE, kJ mol^{-1}) for the internal H-shift step, showing QM and MM contributions

	QM	MM	ONIOM
TS6	167.93 (169.81)[a]	22.03	189.96 (191.83)
TS9	148.49 (150.83)	18.01	166.50 (168.84)
ΔE[b]	39.46 (47.90)	16.53	55.98 (64.43)
ΔE[c]	32.64 (30.66)	7.71	40.35 (38.37)

[a] Energy values in parentheses were obtained at the M06-2X level

[b] Energy values refer to the reaction energy for the formation of ethene

[c] Energy values refer to the reaction energy for the formation of propene

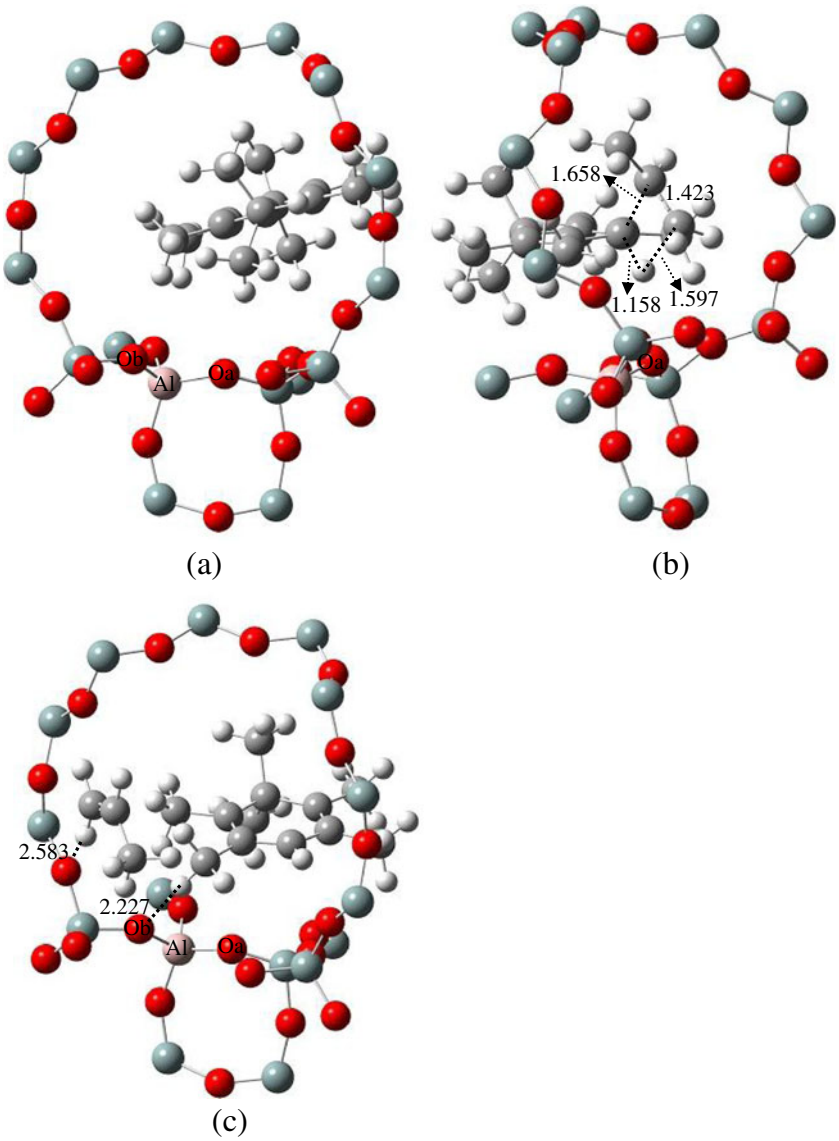

Fig. 10 Optimized structures of **a** INT-8, **b** TS9, and **c** INT-6 with propene

Upon comparing the H-shift step of TS9 during propene production with the H-shift step of TS6 during ethene production (Table 5), it is apparent that the activation barrier of 166.50 kJ mol^{-1} and the reaction energy of 40.35 kJ mol^{-1} for propene are lower than those of ethene (189.96 and 55.98 kJ mol^{-1}, respectively), so the more thermodynamically and kinetically favorable propene is predicted as the major product, which is in accord with experimental observations. The lower activation barrier of TS9 during propene production may be attributed to the stability of the transition state structure. Actually, TS9 and TS6 can form during the reaction of INT-6 with propene and ethene, respectively. In this case, the propene and ethene are protonated by the aromatic H atom of INT-6 to form the secondary and primary hydrocarbon cation fragments of TS9 and TS6, respectively. The more stable secondary hydrocarbon cation fragment of TS9 leads to a lower reaction barrier to propene production.

Completion of the catalytic cycle

The same intermediate, INT-6, is formed during both propene and ethene production. In order to complete the catalytic cycle, the HMB and PMB can be regenerated by performing several successive methyl shift steps (TS10, TS11, and TS12) from the INT-6. The energy data for these transition states are listed in Table 6 and Fig. 2c. The calculated activation barriers for the methyl shifts on the aromatic ring are in the range 64.77–5.04 kJ mol^{-1}, which is in accord with the results of previous theoretical studies [11]. For these reaction barriers, the MM contributions are small, probably because the methyl shift steps are simple unimolecular reactions. After TS12, the intermediate hexaMB$^+$ ion (INT-1) is formed. The structures of TS10–12 and INT-1 are shown in Fig. S2 of the ESM. The distances between the CH_3^+ group and the nearest-neighbor aromatic carbon atom range from 1.854 to 1.972 Å. For each transition state, the CH_3^+ group is located between the acidic site of zeolite and the PMB fragment of TS10–12.

The resulting hexaMB$^+$ ion can lose a proton from the aromatic ring and finally regenerate HMB via the transition state TS2, with an activation barrier of 60.84 kJ mol^{-1}. Another choice is demethylation of the hexaMB$^+$ ion with the co-adsorbed H_2O through TS1, producing PMB and methanol. However, the corresponding activation barrier of 122.53 kJ mol^{-1} is higher than that of TS2, indicating that the regeneration of PMB is more difficult. Because these methyl shifts and deprotonation barriers are lower than those of the rate-determining steps in the production of propene and ethene, the HMB can easily be regenerated in the cage of the H-beta zeolite.

Table 6 Activation barriers (kJ mol^{-1}) of the internal CH_3-shift steps for TS10, TS11, and TS12, showing QM and MM contributions

	QM	MM	ONIOM
TS10	87.62 (89.13)[a]	−2.32	85.30 (86.81)
TS11	67.17 (80.65)	−2.40	64.77 (78.26)
TS12	102.72 (105.24)	−7.68	95.04 (97.56)

[a] Energy values in parentheses were obtained at the M06-2X level

In summary, four different types of reactions are involved in the entire catalytic cycle pathway for the MTP reaction in H-beta zeolite. Their activation barriers decrease in the following order: internal H-shift>methylation>unimolecular CH_3-shift≥deprotonation (Tables 3, 4, 5, and 6). Methylation of the exocyclic double bond is easier than methylation of the ring carbons on the aromatic benzene derivative. Furthermore, in-depth analysis of the energy components of the activation barriers suggests that the MM contribution is negative for methylation and unimolecular CH_3-shift steps but positive for internal H-shift and deprotonation steps. This result indicates that the environment of the framework is more favorable for the formation of the transition states of the former two steps than those of the latter two steps.

Conclusions

In this work, two-layer ONIOM calculations were carried out to investigate the MTP conversion reaction that is catalyzed by H-beta zeolite via the so-called side-chain hydrocarbon pool mechanism. The catalytic cycle starts with the methylation of PMB species, which is followed by deprotonation, methylation, internal H-shift, and CH_3-shift reactions to produce propene and ethene. Finally, the acidic zeolite and HMB are regenerated through several successive methyl shift steps.

The adsorbed methanol is not protonated at the acidic site of the H-beta zeolite. However, the co-adsorption of large molecules such as HMB, HMMC, and HMEC results in the protonation of methanol to $CH_3OH_2^+$, which has two almost equally long O–H distances. The corresponding complex-3, complex-4, and complex-5 are structurally similar to TS3, TS5, and TS8, respectively, which facilitates the formation of transition states. Additionally, comparison of the energy data obtained using the M06-2X and MP2 levels suggests that MP2 electron correlation predicts lower adsorption energies and activation barriers.

The HMMC can be formed by the deprotonation of heptaMB$^+$ ion, and the reverse reaction—the protonation of HMMC—can also easily occur due to its low activation barrier and moderate exothermicity. This result indicates that HMMC and heptaMB$^+$ are in equilibrium, which is in accord with related experimental observations. In particular, for the

first time, Li et al. recently observed the heptaMB$^+$ ion directly under real working conditions on the DNL-6 molecular sieve.

Propene and ethene can be produced by eliminating side ethyl and isopropyl groups of the benzenium ions INT-8 and INT-5, respectively, via an internal H-shift step. The internal H-shift reaction is rate-determining for the MTP catalytic cycle. The calculated results suggest that PMB/H-beta selectively produce propene rather than ethene, based on both kinetic and thermodynamic considerations, which agrees well with experimental results. The more stable secondary hydrocarbon cation fragment in the transition state structure explains the lower reaction barrier for propene production.

Four different types of reactions are involved in the MTP process. Comparison of the activation barriers suggests that they decrease in the following order: internal H-shift> methylation>unimolecular CH_3-shift≥deprotonation. Furthermore, methylation of the exocyclic double bond is easier than methylation of the ring carbons on the aromatic benzene derivative. This indicates that elimination and additive reactions such as internal H-shift and methylation steps are relatively difficult, whereas deprotonation and unimolecular reactions such as CH_3-shift steps are relatively easy.

Decomposing the ONIOM energy into QM and MM contributions is an important way to analyze the effect of the zeolite framework on the reaction steps and product selectivity. The activation barrier data suggest that the MM energy values are negative for methylation and unimolecular CH_3-shift steps but positive for internal H-shift and deprotonation steps. This result implies that the environment of the framework of the H-beta zeolite can stabilize the transition states of the former two steps more efficiently than those of the latter two steps.

Acknowledgments This work was funded by the National Science Foundation of China (nos. 21203118), the Training Program for Young College Teachers in Shanghai (ZZyyy12005), and the Scientific Research Foundation of Shanghai Institute of Technology (grant YJ2012-11).

References

1. Stöcker M (1999) Microporous Mesoporous Mater 29:3–48
2. Ladwig PK, Asplin JE, Stuntz GF, Wachter WA, Henry BE (2000) US Patent 6,069,287 (assigned to Exxon Research and Engineering Corporation)
3. Svelle S, Olsbye U, Joensen F, Bjørgen M (2007) J Phys Chem C 111:17981–17984
4. Song WG, Haw JF, Nicholas JB, Heneghan CS (2000) J Am Chem Soc 122:10726–10727
5. Sassi A, Wildman MA, Ahn HJ, Prasad P, Nicholas JB, Haw JF (2002) J Phys Chem B 106:2294–2303
6. Bjørgen M, Bonino F, Kolboe S, Lillerud KP, Zecchina A, Bordiga S (2003) J Am Chem Soc 125:15863–15868
7. Svelle S, Joensen F, Nerlov J, Olsbye U, Lillerud KP, Kolboe S, Bjørgen M (2006) J Am Chem Soc 128:14770–14771
8. Arstad B, Kolboe S, Swang O (2002) J Phys Chem B 106:12722–12726
9. Arstad B, Nicholas JB, Haw JF (2004) J Am Chem Soc 126:2991–3001
10. Vos AM, Rozanska X, Schoonheydt RA, van Santen RA, Hutschka F, Hafner J (2001) J Am Chem Soc 123:2799–2809
11. Wang CM, Wang YD, Xie ZK, Liu ZP (2009) J Phys Chem C 113:4584–4591
12. Boronat M, Viruela PM, Corma A (2004) J Am Chem Soc 126:3300–3309
13. Nieminen V, Sierka M, Murzin DY, Sauer J (2005) J Catal 231:393–404
14. Joshi YV, Thomson KT (2005) J Catal 230:440–463
15. Vreven T, Morokuma K (2000) J Comput Chem 21:1419–1432
16. Vreven T, Mennucci B, da Silva CO, Morokuma K, Tomasi J (2001) J Chem Phys 115:62–72
17. Vreven T, Byun KS, Komaromi I, Dapprich S, Montgomery JA, Morokuma K, Frisch MJ (2006) J Chem Theory Comput 2:815–826
18. Lesthaeghe D, Sterck BD, Speybroeck VV, Marin GB, Waroquier M (2007) Angew Chem Int Ed 46:1311–1314
19. Mynsbrugge JVD, Visur M, Olsbye U, Beato P, Bjørgen M, Speybroeck VV, Svelle S (2012) J Catal 292:201–212
20. Sun YX, Yang J, Zhao LF, Dai JX, Sun H (2010) J Phys Chem C 114:5975–5984
21. Newsam JM, Treacy MMJ, Koetsier WT, der Gruyter CB (1988) Proc R Soc Lond A 420:375–405
22. Maseras F, Morokuma K (1995) J Comput Chem 16:1170–1179
23. Morokuma K (2003) Bull Korean Chem Soc 24:797–801
24. Zhao Y, Truhlar DG (2008) J Phys Chem C 112:6860–6868
25. Zhao Y, Truhlar DG (2008) Acc Chem Res 41:157–167
26. Zhao Y, Schultz NE, Truhlar DG (2006) J Chem Theory Comput 2:364–382
27. Zhao Y, Truhlar DG (2008) Theor Chem Accounts 120:215–241
28. Rappe AK, Casewit CJ, Colwell KS, Goddard WA III, Skiff WM (1992) J Am Chem Soc 114:10024–10035
29. Becke AD (1993) J Chem Phys 98:5648–5652
30. Kumsapaya C, Bobuatong K, Khongpracha P, Tantirungrotechai Y, Limtrakul J (2009) J Phys Chem C 113:16128–16137
31. Heinz H, Suter UW (2004) J Phys Chem B 108:18341–18352
32. Asada N, Fedorov DG, Kitaura K, Nakanishi I, Merz KM Jr (2012) J Phys Chem Lett 3:2604–2610
33. Otsuka M, Tsuchida N, Ikeda Y, Kimura Y, Mutoh Y, Ishii Y, Takano K (2012) J Am Chem Soc 134:17746–17756
34. Li X, Chung LW, Paneth P, Morokuma K (2009) J Am Chem Soc 131:5115–5125
35. Frisch MJ, Trucks GW, Schlegel HB, Scuseria GE, Robb MA, Cheeseman JR, Scalmani G, Barone V, Mennucci B, Petersson GA, Nakatsuji H, Caricato M, Li X, Hratchian HP, Izmaylov AF, Bloino J, Zheng G, Sonnenberg JL, Hada M, Ehara M, Toyota K, Fukuda R, Hasegawa J, Ishida M, Nakajima T, Honda Y, Kitao O, Nakai H, Vreven T, Montgomery JA Jr, Peralta JE, Ogliaro F, Bearpark M, Heyd JJ, Brothers E, Kudin KN, Staroverov VN, Kobayashi R, Normand J, Raghavachari K, Rendell A, Burant JC, Iyengar SS, Tomasi J, Cossi M, Rega N, Millam NJ, Klene M, Knox JE, Cross JB, Bakken V, Adamo C, Jaramillo J, Gomperts R, Stratmann RE, Yazyev O, Austin AJ, Cammi R, Pomelli C, Ochterski JW, Martin RL, Morokuma K, Zakrzewski VG, Voth GA, Salvador P, Dannenberg JJ, Dapprich S, Daniels AD, Farkas Ö, Foresman JB, Ortiz JV, Cioslowski J, Fox DJ (2009) Gaussian 09, revision A.01. Gaussian, Inc., Wallingford
36. Hill IM, Hashimi SA, Bhan A (2012) J Catal 285:115–123
37. Svelle S, Visur M, Olsbye U, Saepurahman S, Bjørgen M (2011) Top Catal 54:897–906
38. Maihom T, Boekfa B, Sirijaraensre J, Nanok T, Probst M, Limtrakul J (2009) J Phys Chem C 113:6654–6662

39. Saepurahman S, Visur M, Olsbye U, Bjørgen M, Svelle S (2011) Top Catal 54:1293–1301
40. Svelle S, Tuma C, Rozanska X, Kerber T, Sauer J (2009) J Am Chem Soc 131:816–825
41. Doering W v E, Saunders M, Boyton HG, Earhart HW, Wadley EF, Edwards WR, Laber G (1958) Tetrahedron 4:178–185
42. Li JZ, Wei YX, Chen JR, Tian P, Su X, Xu S, Qi Y, Wang QY, Zhou Y, He YL, Liu ZM (2012) J Am Chem Soc 134:836–839